2018 Annual American Control Conference (ACC)
June 27–29, 2018. Wisconsin Center, Milwaukee, USA

Suppressing Chaotic and Hyperchaotic Dynamics of Smart Valves Network Using A Centralized Adaptive Approach

Peiman Naseradinmousavi[1], Hashem Ashrafiuon[2], and Mostafa Bagheri[3]

***Abstract*— Catastrophic chaotic and hyperchaotic dynamical behavior have been experimentally observed in the so-called "Smart Valves" network, given certain critical parameters and initial conditions. The centralized network-based control of these coupled systems may effectively mitigate the harmful dynamics of the valve-actuator configuration which can be potentially caused by a remote set and would gradually affect the whole network. In this work, we address the centralized control of two bi-directional solenoid actuated butterfly valves dynamically coupled in series subject to the chaotic and hyperchaotic dynamics. An interconnected adaptive scheme is developed and examined to vanish both the chaotic and hyperchaotic dynamics and return the coupled network to its safe domain of operation.**

I. Introduction

Dangerous dynamical behaviors of multidisciplinary systems, in particular the electromechanical ones, need to be controlled in order to avoid the expected failure of the large-scale network. The so-called "Smart Valves" network, containing many interconnected electro-magneto-mechanical-fluid components, plays an important role in proper and efficient performance of many critical infrastructures which include, but are not limited to, municipal piping systems, oil and gas fields, petrochemical plants, and the US Navy. A robust control scheme is hence required to mitigate the effects of the harmful dynamic responses in the presence of uncertainties involved with such a large-scale network.

We have reported broad analytical and experimental studies [1]–[15] for both an isolated actuator-valve arrangement and a network of two interconnected solenoid actuated butterfly valves operating in series. Finding specific research work to capture and control the chaotic and hyperchaotic dynamics of such a multiphysics network is somewhat difficult although some efforts have been reported for similar case studies. Wan and Jian [16] have studied gear dynamics with turbulent journal bearings mounted hybrid squeeze film damper. In order to avoid the nonsynchronous chaotic vibrations, they utilized an increased proportional gain $K_p = 0.1$ to control this system. It was shown that the pinion trajectory will leave chaotic motion to periodic motion in the steady state under control action. Morel *et al.* [17] proposed a new nonlinear feedback, which induces chaos and which was able at the same time to achieve a low spectral emission and to maintain a small ripple in the output. The design of this new and simple controller was based on the propriety that chaotified nonlinear systems present many independent chaotic attractors of small dimensions. Chen and Liu [18] investigated chaos control of fractional-order energy demand-supply system by two different control strategies: a linear feedback control and an adaptive switching control strategy via a single control input. Some other efforts related to the chaos control can be found in [19]–[22].We here briefly represent the interconnected analytical model of two sets (for completeness) along with the critical initial conditions and parameters resulted in the dangerous responses. The coupled adaptation and control laws will be formulated with respect to the interconnected dynamics of the system. The results will be thoroughly discussed to address the robustness of adaptive scheme for vanishing the chaotic and hyperchaotic dynamics.

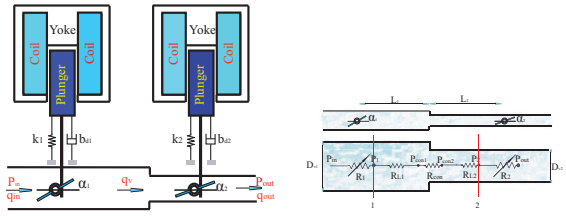

Fig. 1. (a) A schematic configuration of two bi-directional solenoid actuated butterfly valves subject to the sudden contraction; (b) A coupled model of two butterfly valves in series without actuation

II. Mathematical Modeling

The system, which is being considered here, is two bi-directional solenoid actuated butterfly valves operating in series. The system undergoes a sudden pipe contraction as shown in Fig 1. The plungers are connected to the valves' stems through the rack and pinion arrangements yielding kinematic constraints. We have previously derived the interconnected analytical model of two sets operating in series [2]–[9] and briefly represent here for completeness. As can be observed in Fig. 1(b), the valves are modeled as changing resistors:

$$R_{ni}(\alpha_i) = \frac{e_i}{(p_i\alpha_i^3 + q_i\alpha_i^2 + o_i\alpha_i + \gamma_i)^2}, (i = 1, 2) \quad (1)$$

where, R_{n1} and R_{n2} indicate the resistances of the upstream and downstream valves, respectively, and $e_1 = 7.2 \times 10^5$, $p_1 = 461.9$, $q_1 = -405.4$, $o_1 = -1831$, $\gamma_1 = 2207$, $e_2 = 4.51 \times 10^5$, $p_2 = 161.84$, $q_2 = -110.53$, $o_2 =$

[1]Peiman Naseradinmousavi is with the Department of Mechanical Engineering, San Diego State University, San Diego, CA 92115, USA http://peimannm.sdsu.edu
[2]Hashem Ashrafiuon is with the Department of Mechanical Engineering, Villanova University, Villanova, PA 19085, USA http:/homepage.villanova.edu/hashem.ashrafiuon/
[3]Mostafa Bagheri is with the Department of Mechanical and Aerospace Engineering, San Diego State University and University of California San Diego, USA. http://peimannm.sdsu.edu/members.html

-695.1, and $\gamma_2 = 807.57$ for two different valves' diameters. Also the flow between the valves in addition to the sudden contraction are modeled as constant resistors based on the Hagen-Poiseuille and Borda-Carnot formulas:

$$R_{Li} = \frac{128\mu_f L_i}{\pi D_{vi}^4}, \ (i = 1, 2) \tag{2}$$

$$R_{con} = \frac{8K_{con}}{\pi^2 D_{v2}^4} \tag{3}$$

where, $K_{con} = 0.5(1-\beta^2)\sqrt{\sin\left(\frac{\theta}{2}\right)}$, β indicates the ratio of minor and major diameters $\left(\frac{D_{v2}}{D_{v1}}\right)$, θ is the angle of approach (the pipe contraction angle), μ_f stands for the fluid dynamic viscosity, D_{v1} and D_{v2} are the upstream and downstream valves' diameters, respectively, L_1 and L_2 indicate the pipe lengths before and after contraction, and R_{L1} and R_{L2} are the constant resistances. Therefore, two valves operating in series can be modeled as a set of five resistors leading us to derive mathematical expressions of the pressures after and before the upstream and downstream valves, respectively, as follows.

$$P_1 = \frac{R_{n2}P_{in} + R_{n1}P_{out} + R_{n1}(R_{L1} + R_{L2} + R_{con}q_v)q_v}{(R_{n1} + R_{n2})} \tag{4}$$

$$P_2 = \frac{R_{n2}P_{in} + R_{n1}P_{out} - R_{n2}(R_{L1} + R_{L2} + R_{con}q_v)q_v}{(R_{n1} + R_{n2})} \tag{5}$$

where q_v is the volumetric flow rate. These interconnected pressures were used in developing both the coupled hydrodynamic and bearing torques [2], [3]:

$$\begin{aligned} T_{h1} &= (a_1\alpha_1 e^{b_1{\alpha_1}^{1.1}} - c_1 e^{d_1\alpha_1})(P_{in} - P_1) \\ &= (a_1\alpha_1 e^{b_1{\alpha_1}^{1.1}} - c_1 e^{d_1\alpha_1}) \times \frac{\frac{e_1}{(p_1\alpha_1^3+q_1\alpha_1^2+o_1\alpha_1+\gamma_1)^2}}{\sum_{i=1}^{2}\frac{e_i}{(p_i\alpha_i^3+q_i\alpha_i^2+o_i\alpha_i+\gamma_i)^2}} \\ &\times \ (P_{in} - P_{out} - (R_{L1} + R_{L2} + R_{con}q_v)q_v) \end{aligned} \tag{6}$$

$$\begin{aligned} T_{h2} &= (a_1'\alpha_2 e^{b_1'{\alpha_2}^{1.1}} - c_1' e^{d_1'\alpha_2})(P_2 - P_{out}) \\ &= (a_1'\alpha_2 e^{b_1'{\alpha_2}^{1.1}} - c_1' e^{d_1'\alpha_2}) \times \frac{\frac{e_2}{(p_2\alpha_2^3+q_2\alpha_2^2+o_2\alpha_2+\gamma_2)^2}}{\sum_{i=1}^{2}\frac{e_i}{(p_i\alpha_i^3+q_i\alpha_i^2+o_i\alpha_i+\gamma_i)^2}} \\ &\times \ (P_{in} - P_{out} - (R_{L1} + R_{L2} + R_{con}q_v)q_v) \end{aligned} \tag{7}$$

$$T_{b1} = C_1\Delta P_1(R_{n1}, R_{n2}, R_{L1}, R_{L2}, R_{con}) \tag{8}$$

$$T_{b2} = C_2\Delta P_2(R_{n1}, R_{n2}, R_{L1}, R_{L2}, R_{con}) \tag{9}$$

where, $a_1 = 0.4249$, $a_1' = 0.1022$, $b_1 = -18.52$, $b_1' = -17.0795$, $c_1 = -7.823 \times 10^{-4}$, $c_1' = -2 \times 10^{-4}$, $d_1 = -1.084$, $d_1' = -1.0973$, $C_1 = C_2 = 0.5A_d\mu D_s$, $\Delta P_1 = P_{in} - P_1$, $\Delta P_2 = P_2 - P_{out}$, and P_{in} and P_{out} are the given inlet and outlet pressures, respectively. Note that D_s is the stem diameter of the valve and μ stands for the friction coefficient of the bearing area. We have previously established that the hydrodynamic torque acts as a helping load pushing the valve to be closed and is typically effective for when the valve angle is lower than 60° [3], [5]; the effective range was experimentally examined [5] confirming the helping behavior of the hydrodynamic torque by presenting positive values. The bearing torque, due to its friction-based nature, always acts as a resisting load. Based on the analytical formulas addressed above, the sixth-order interconnected dynamic equations of two bi-directional

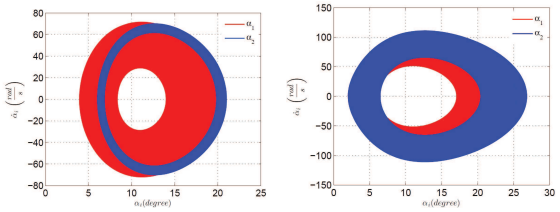

(a) (b)

Fig. 2. (a) The coupled sets' phase portraits for Initial$_1$; (b) The coupled sets' phase portraits for Initial$_2$

solenoid actuated butterfly valves were developed as follows:

$$\dot{z}_1 = z_2 \tag{10}$$

$$\begin{aligned} \dot{z}_2 = \frac{1}{J_1}\Bigg[&\frac{r_1 C_{21} N_1^2 z_3^2}{2(C_{11} + C_{21}(g_{m1} - r_1 z_1))^2} - b_{d1}z_2 - k_1 z_1 \\ + \ &\frac{\frac{(P_{in} - P_{out} - (R_{L1}+R_{L2}+R_{con}q_v)q_v)e_1}{(p_1 z_1^3+q_1 z_1^2+o_1 z_1+\gamma_1)^2}}{\sum_{i=1,4}\frac{e_i}{(p_i z_i^3+q_i z_i^2+o_i z_i+\gamma_i)^2}} \times \\ &\left[(a_1 z_1 e^{b_1{z_1}^{1.1}} - c_1 e^{d_1 z_1}) - C_1 \times \tanh(K z_2)\right]\Bigg] \end{aligned} \tag{11}$$

$$\begin{aligned} \dot{z}_3 = &\frac{(V_1 - R_1 z_3)(C_{11} + C_{21}(g_{m1} - r_1 z_1))}{N_1^2} - \\ &\frac{r_1 C_{21} z_3 z_2}{(C_{11} + C_{21}(g_{m1} - r_1 z_1))} \end{aligned} \tag{12}$$

$$\dot{z}_4 = z_5 \tag{13}$$

$$\begin{aligned} \dot{z}_5 = \frac{1}{J_2}\Bigg[&\frac{r_2 C_{22} N_2^2 z_6^2}{2(C_{12} + C_{22}(g_{m2} - r_2 z_4))^2} - b_{d2}z_5 - k_2 z_4 \\ + \ &\frac{\frac{(P_{in} - P_{out} - (R_{L1}+R_{L2}+R_{con}q_v)q_v)e_2}{(p_2 z_4^3+q_2 z_4^2+o_2 z_4+\gamma_2)^2}}{\sum_{i=1,4}\frac{e_i}{(p_i z_i^3+q_i z_i^2+o_i z_i+\gamma_i)^2}} \times \\ &\left[(a_1' z_4 e^{b_1'{z_4}^{1.1}} - c_1' e^{d_1' z_4}) - C_2 \times \tanh(K z_5)\right]\Bigg] \end{aligned} \tag{14}$$

$$\begin{aligned} \dot{z}_6 = &\frac{(V_2 - R_2 z_6)(C_{12} + C_{22}(g_{m2} - r_2 z_4))}{N_2^2} - \\ &\frac{r_2 C_{22} z_5 z_6}{(C_{12} + C_{22}(g_{m2} - r_2 z_4))} \end{aligned} \tag{15}$$

where, b_{di} indicates the equivalent torsional damping, k_i is the equivalent torsional stiffness, V_i stands for the supply voltage, r_i indicates the radius of the pinion, C_1 and C_2 are the reluctances of the magnetic path without air gap and that of the air gap, respectively, N_i stands for the number of coils, g_{mi} is the nominal air gap, J_i indicates the polar moment of inertia of the valve's disk, and R_i is the electrical resistance of coil. $z_1 = \alpha_1$, $z_2 = \dot{\alpha}_1$, and $z_3 = i_1$ indicate the upstream valve's rotation angle, angular velocity, and actuator current, respectively. $z_4 = \alpha_2$, $z_5 = \dot{\alpha}_2$, and $z_6 = i_2$ stand for the downstream valve's rotation angle, angular velocity, and actuator current, respectively. The network parameters are listed in Table I.

Note that we could capture, for the first time, the coupled chaotic and hyperchaotic dynamics of the interconnected sets [2] by examining the critical values of $b_{di} =$

TABLE I

THE SYSTEM PARAMETERS

ρ	$1000\frac{kg}{m^3}$	v	$3\frac{m}{s}$
$J_{1,2}$	$0.104 \times 10^{-1}(kg.m^2)$	N_2	3300
N_1	3300	$C_{11,22}$	1.56×10^6
D_{v1}	0.2032(m)	D_{v2}	0.127(m)
$D_{s1,s2}$	0.01(m)	P_{out}	2(kPa)
$k_{1,2}$	$60(N.m^{-1})$	$C_{21,22}$	6.32×10^8
L_1	2(m)	L_2	1(m)
$r_{1,2}$	0.05(m)	θ	90°
P_{in}	256(kPa)	$g_{m1,m2}$	0.1(m)
μ_f	0.018 $(Kg.m^{-1}.s^{-1})$	$\lambda_{1,2}$	1
$n_{1,2}$	10	$b_{di} = \mu_i$	1×10^{-7}

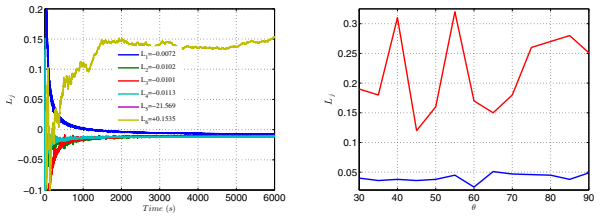

(a) (b)

Fig. 3. (a) The Lyapunov exponents for Initial$_1$; (b) The positive Lyapunov exponents for Initial$_2$ vs. different approach angles (θ)

$\mu_i = 1 \times 10^{-7}$ for two different initial conditions of Initial$_1$ = $[20(deg)\ 0\ 0\ 20(deg)\ 0\ 0]$ and Initial$_2$ = $[2(deg)\ 0\ 0\ 2(deg)\ 0\ 0]$, respectively. Shown in Figs. 2(a) and 2(b) are the chaotic and hyperchaotic dynamics of the coupled actuated valves, respectively; the red and blue lines indicate the angular velocities vs. rotation angles of the upstream and downstream valves, respectively. Some powerful tools of the nonlinear analysis, including the Lyapunov exponents and Poincaré map, were used in distinguishing among the nature of harmful responses, as shown in Figs. 3(a) & 3(b). One and two positive Lyapunov exponents along with irregular Poincaré maps confirmed [2] the chaotic and hyperchaotic dynamics of the actuated valves, respectively. Such dangerous responses need to be vanished using a nonlinear control scheme, due to the nonlinear and coupled nature of the network, in order to return the interconnected sets to their stable domains. The operationally optimized valves' motions, on the other hand, are utilized in the nonlinear control scheme as desirable trajectories. Based on the inevitable unknown parameters of such a coupled network, the nonlinear model-based adaptive scheme looks as an effective approach to be employed in stabilizing the system subject to the chaotic and hyperchaotic dynamics.

III. CONTROL AND ADAPTATION LAWS

The nonlinear model-based adaptive control method [23], [24] is used in stabilizing the unstable system in order to track the desired trajectories [2], [4] defined based on the critical initial conditions as follows:

$$\alpha_{di} = \frac{\pi}{3}\tanh(10^{-4}t^3) + \frac{\pi}{9},\ \text{Initial}_1 \quad (16)$$

$$\alpha_{di} = \frac{\pi}{3}\tanh(10^{-4}t^3) + \frac{\pi}{90},\ \text{Initial}_2 \quad (17)$$

The so-called "S-Shaped" trajectories are highly energy-efficient [4] and yield smooth dynamic responses avoiding the repeatedly observed dangerous phenomenon of "Water Hammering". The coupled dynamic Eqs. 11 and 14 can be rewritten as the following:

$$J_i\ddot{\alpha}_i + b_{di}\dot{\alpha}_i + k_i\alpha_i = \frac{r_i C_{2i} N_i^2 i_i^2}{2(C_{1i} + C_{2i}(g_{mi} - r_i\alpha_i))^2} + \frac{A_1 R_{ni}}{\sum_{i=1}^{2} R_{ni}}[T'_{hi} - T'_{bi}\tanh(K\dot{\alpha}_i)],\ (i = 1, 2) \quad (18)$$

where, $A_1 = (P_{in} - P_{out} - (R_{L1} + R_{L2} + R_{con}q_v)q_v)$, $T'_{h1} = a_1\alpha_1 e^{b_1{\alpha_1}^{1.1}} - c_1 e^{d_1\alpha_1}$, $T'_{h2} = a'_1\alpha_2 e^{b'_1{\alpha_2}^{1.1}} - c'_1 e^{d'_1\alpha_2}$, $T'_{b1} = C_1$, and $T'_{b2} = C_2$. Assuming,

$$M_i = \frac{2J_i(C_{i1} + C_{2i}(g_{mi} - r_i\alpha_i))^2}{r_i C_{2i} N_i^2},\ B_i = \frac{2b_{di}(C_{i1} + C_{2i}(g_{mi} - r_i\alpha_i))^2}{r_i C_{2i} N_i^2}$$

$$K_i = \frac{2k_i(C_{i1} + C_{2i}(g_{mi} - r_i\alpha_i))^2}{r_i C_{2i} N_i^2},\ Co_i = \frac{2(C_{i1} + C_{2i}(g_{mi} - r_i\alpha_i))^2}{r_i C_{2i} N_i^2}$$

Eq. 18 can be rewritten as follows.

$$M_i\ddot{\alpha}_i + B_i\dot{\alpha}_i + K_i\alpha_i = u_i + \frac{A_1 Co_i R_{ni}}{\sum_{i=1}^{2} R_{ni}}[T'_{hi} - T'_{bi}\tanh(K\dot{\alpha}_i)],\ (i = 1, 2) \quad (19)$$

We define the valves' tracking errors and their first and second time derivatives as the following:

$$e_i = \alpha_{di} - \alpha_i, \dot{e}_i = \dot{\alpha}_{di} - \dot{\alpha}_i, \ddot{e}_i = \ddot{\alpha}_{di} - \ddot{\alpha}_i,\ (i = 1, 2)$$

This yields,

$$M_i\ddot{e}_i = M_i\ddot{\alpha}_{di} - M_i\ddot{\alpha}_i = M_i\ddot{\alpha}_{di} + B_i\dot{\alpha}_i + K_i\alpha_i - u_i - \frac{A_1 Co_i R_{ni}}{\sum_{i=1}^{2} R_{ni}}[T'_{hi} - T'_{bi}\tanh(K\dot{\alpha}_i)],\ (i = 1, 2) \quad (20)$$

The combined tracking errors [23], [24] and their first time derivatives are as follows:

$$s_i = \dot{e}_i + \lambda_i e_i, \dot{s}_i = \ddot{e}_i + \lambda_i\dot{e}_i,\ (i = 1, 2)$$

where λ's are strictly positive numbers listed in Table I. Premultiplying by M_i and substituting from Eq. 20, we have,

$$M_i\dot{s}_i = M_i\ddot{\alpha}_{di} + B_i\dot{\alpha}_i + K_i\alpha_i - u_i - \frac{A_1 Co_i R_{ni}}{\sum_{i=1}^{2} R_{ni}}[T'_{hi} - T'_{bi}\tanh(K\dot{\alpha}_i)] + M_i\lambda_i\dot{e}_i \quad (21)$$

Based on the interconnected dynamics of the network, we chose the following quadratic Lyapunov function candidate:

$$V = \frac{1}{2}\left[\sum_{i=1}^{2}(s_i^T M_i s_i + \tilde{\Theta}_i^T\Gamma_i^{-1}\tilde{\Theta}_i)\right] \quad (22)$$

where Γ_i is a symmetric positive definite matrix and $\tilde{\Theta}_i$ is the system's lumped parameter estimation error ($\tilde{\Theta}_i = \Theta_i - \hat{\Theta}_i$). Differentiating the Lyapunov function (Eq. 22) yields,

$$\dot{V} = \sum_{i=1}^{2}(s_i^T M_i\dot{s}_i + \frac{1}{2}s_i^T\dot{M}_i s_i - \tilde{\Theta}_i^T\Gamma_i^{-1}\dot{\hat{\Theta}}_i)$$

$$= \sum_{i=1}^{2}\left[s_i^T\left[M_i\ddot{\alpha}_{di} + B_i\dot{\alpha}_i + K_i\alpha_i - u_i - \frac{A_1 Co_i R_{ni}}{\sum R_{ni}}\right.\right.$$

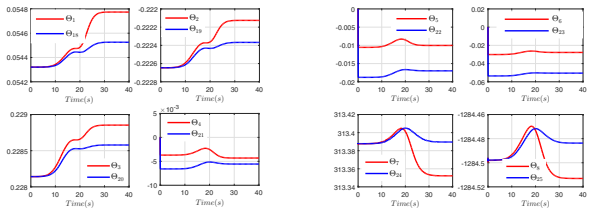

(a) (b)

Fig. 4. The parameter estimation for Θ_1 to Θ_8 of the upstream set and Θ_{18} to Θ_{25} of the downstream set.

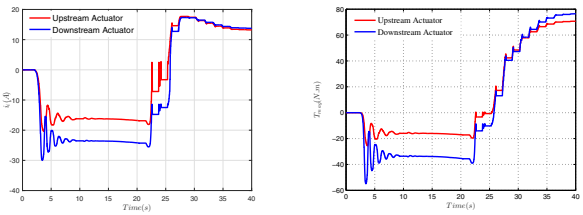

(a) (b)

Fig. 5. (a) The control inputs; (b) The magnetic torques

$$\times \quad [T'_{hi} - T'_{bi}\tanh(K\dot{\alpha}_i)] + M_i\lambda_i\dot{e}_i + \frac{1}{2}\dot{M}_i s_i\Big] - \tilde{\Theta}_i^T\Gamma_i^{-1}\dot{\hat{\Theta}}_i\Big] \tag{23}$$

By defining the regression vectors as the following:

$$W_i\Theta_i = M_i\ddot{\alpha}_{di} + B_i\dot{\alpha}_i + K_i\alpha_i - \frac{A_1 Co_i R_{ni}}{\sum R_{ni}} \times \quad [T'_{hi} - T'_{bi}\tanh(K\dot{\alpha}_i)] + M_i\lambda_i\dot{e}_i + \frac{1}{2}\dot{M}_i s_i, \ (i = 1, 2) \tag{24}$$

The $\dot{V}$ can be easily rewritten as follows.

$$\dot{V} = \sum_{i=1}^{2}\left[s_i^T[W_i\Theta_i - u_i] - \tilde{\Theta}_i^T\Gamma_i^{-1}\dot{\hat{\Theta}}_i\right] \tag{25}$$

The appropriate control inputs are hence chosen as the following:

$$u_i = W_i\hat{\Theta}_i + n_i s_i, \ (i = 1, 2) \tag{26}$$

where,

$$W_i\hat{\Theta}_i = \hat{M}_i\ddot{\alpha}_{di} + \hat{B}_i\dot{\alpha}_i + \hat{K}_i\alpha_i - \frac{A_1\hat{Co}_i R_{ni}}{\sum R_{ni}} \times [T'_{hi} - T'_{bi}\tanh(K\dot{\alpha}_i)] + \hat{M}_i\lambda_i\dot{e}_i + \frac{1}{2}\hat{M}_i s_i, \ (i = 1, 2) \tag{27}$$

We can easily develop both the regression ($W_i \in \Re^{1\times 17}$) and estimated lumped parameter vectors ($\hat{\Theta}_i \in \Re^{17\times 1}$). Substituting the control inputs into Eq. 25 gives,

$$\begin{aligned}\dot{V} &= \sum_{i=1}^{2} s_i^T[\underbrace{W_i\Theta_i - W_i\hat{\Theta}_i}_{W_i\tilde{\Theta}_i} - n_i s_i] - \tilde{\Theta}_i^T\Gamma_i^{-1}\dot{\hat{\Theta}}_i \\ &= \sum_{i=1}^{2} s_i^T W_i\tilde{\Theta}_i - s_i^T n_i s_i - \tilde{\Theta}_i^T\Gamma_i^{-1}\dot{\hat{\Theta}}_i \\ &= \sum_{i=1}^{2}[s_i^T W_i - \Gamma_i^{-1}\dot{\hat{\Theta}}_i^T]\tilde{\Theta}_i - s_i^T n_i s_i \end{aligned} \tag{28}$$

which leads us to develop the following parameters' adaptation laws:

$$\dot{\hat{\Theta}}_i = \Gamma_i W_i^T s_i \tag{29}$$

Substituting Eq. 29 into Eq. 28 yields,

$$\dot{V} = \sum_{i=1}^{2} -s_i^T n_i s_i \leq 0 \tag{30}$$

Based on Eq. 30, by Lasalle-Yoshizawa theorem, we get that $s_i \to 0$ as $t \to \infty$. This implies by the input-to-state stability property of the system $\dot{e}_i + \lambda_i e_i = s_i$, that e_i and $\dot{e}_i$ tend to zero as $t \to \infty$. We hence guarantee both the global stability of the coupled network (the boundedness of α_i, $\dot{\alpha}_i$, and $\hat{\Theta}_i$) and convergence of the tracking errors (e_i).

IV. Results

The values of n_i used in the coupled control inputs (Eq. 26) are listed in Table I and $\Gamma_i = \text{diag}[10]_{17\times 17}$. Fig. 4 presents the sample estimation process of the unknown parameters (Θ_1–Θ_8) & (Θ_{18}–Θ_{25}) for both the upstream and downstream sets subject to the Initial$_1$ revealing the parameters convergence within the nominal operation time of 40(s); the Initial$_1$ yielded the coupled chaotic dynamics. Note that the initial values of Θ_1–Θ_{34} used in the adaptation laws are 90% of their nominal values. Such initial values are intentionally selected to yield meaningful estimated parameters with respect to the electro-magneto-mechanical-fluid nature of the network. It is of a great interest to observe that, despite the dominant chaotic dynamics resulted from the Initial$_1$, the parameters timely converge and therefore, we expect to observe stable operations of both the coupled actuated valves. Note that this approach, based on the "sufficient richness" condition [23], [24], would not exactly estimate the unknown parameters such that it expectedly yields values to allow the desired task to be carried out.

The estimated parameters, based on Eq. 26, would help generate powerful control inputs, the applied currents of the bi-directional solenoid actuators (i_i), to vanish the chaotic dynamics of the interconnected sets (Fig. 2(a)) and then drive the coupled valves to track the desirable trajectories, which we addressed earlier (Eq. 16). Shown in Fig. 5(a) are the control inputs for both the upstream and downstream actuators. As expected, the currents consist of two phases as shown in Fig. 5(a). The first phase, with oscillatory negative values of the currents, suppresses the coupled chaotic dynamics due to the Initial$_1$ resulting in downward/slightly upward motions of the plungers, which would consequently avoid the sudden jumps of the valves. During the second phase of the control process, the currents gradually take positive values indicating that the plungers move upward and therefore, the valves rotate toward the desirable trajectories.

It is of a great interest to observe that the control input of the downstream set is remarkably higher than that of the upstream one, in particular for the first phase of the control process. The physical interpretation of such higher values of the control input used in the downstream set can be explained through the effects of the flow loads acting on the valve, in

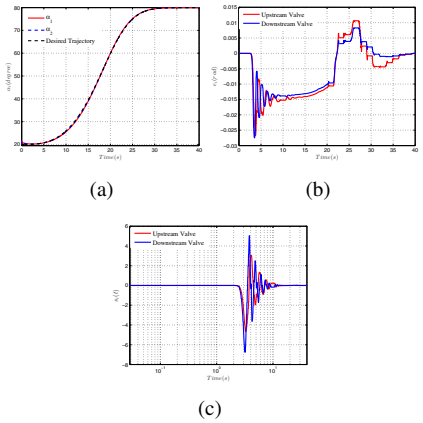

(a) (b)

(c)

Fig. 6. (a) The valves' rotation angles; (b) The error signals; (c) The combined tracking error signals

particular the hydrodynamic torque:

$$\frac{T_{h2}}{T_{h1}} \propto \left(\frac{D_{v2}}{D_{v1}}\right)^3 \times \left(\frac{c_{v1}}{c_{v2}}\right)^2 \quad (31)$$

$$\frac{T_{b2}}{T_{b1}} \propto \left(\frac{D_{v2}c_{v1}}{D_{v1}c_{v2}}\right)^2 \quad (32)$$

where c_{v1} and c_{v2} are the upstream and downstream valves' coefficients, respectively ($c_{vi}(\alpha_i) = p_i\alpha_i^3 + q_i\alpha_i^2 + o_i\alpha_i + \gamma_i$); we have provided the values of p_i, q_i, o_i, and γ_i in Section 2. We have previously reported [2]–[9] that a smaller pipe diameter yields both the higher hydrodynamic and bearing torques due to the higher coefficient of the upstream valve than that of the downstream one (Eqs. 31 and 32). From another aspect, the hydrodynamic torque is a helping load [2]–[9] to close the symmetric valve whereas the bearing one is a resistance (friction-based) torque for the valve's operation. The downstream set with a smaller pipe diameter, subject to the chaotic dynamics of the Initial$_1$, undoubtedly needs more suppressing control input to mitigate the destabilizer effects of the higher hydrodynamic torque acting on the valve. For the second phase of the control process, the higher resistance bearing torque acting on the downstream set inevitably demands slightly higher control input to push the valve to the desirable trajectory.

Such profiles of the control inputs for both the sets are expected to be observed for the driving magnetic torques (forces) as nonlinear functions of the control inputs in addition to the valves' rotation angles/plungers' displacements. Fig. 5(b) presents the driving magnetic torques of both the coupled sets in which the two phases of the control process can be distinguished as we discussed for the currents. The oscillatory negative values of the magnetic torques suppress the chaotic dynamics along with mitigating the effects of the hydrodynamic torques. The positive magnetic torques (forces) move the plungers upward and subsequently, the valves move toward the desirable trajectories. The higher amount of the driving magnetic torque of the downstream set, for the second phase of the control process, looks logical to overcome the higher resistance bearing torque than that of the upstream one.

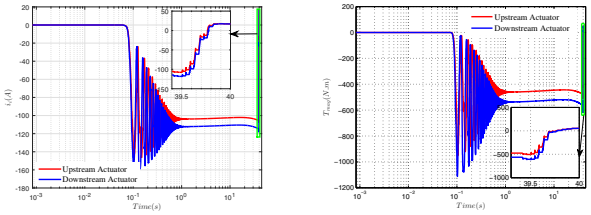

(a) (b)

Fig. 7. (a) The control inputs; (b) The magnetic torques

Shown in Fig. 6(a) are the upstream and downstream valves' rotation angles indicating that both the sets track the desirable trajectories (Eq. 16) by applying the control inputs which expectedly vanish the coupled chaotic dynamics due to the Initial$_1$. Both the error (e_i) and combined tracking error (s_i) signals shown in Figs. 6(b) and 6(c), respectively, converge to zero revealing that the valves' angles (α_i) tend to the desirable trajectories (α_{di}) within the nominal operation time.

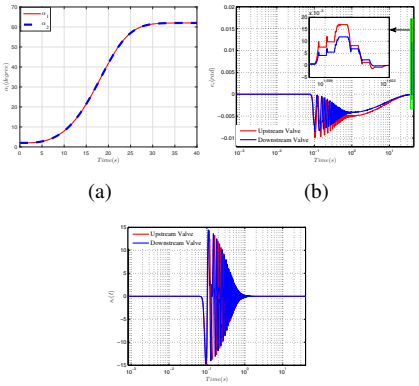

(a) (b)

(c)

Fig. 8. (a) The valves' rotation angles; (b) The error signals; (c) The combined tracking error signals

Figs. 7(a) and 7(b) present the control inputs and driving magnetic torques, respectively, used in vanishing the coupled hyperchaotic dynamics caused by the Initial$_2$ (Fig. 2(b)). As expected, the hyperchaotic dynamics of both the sets with the larger domains of attractions, which we have thoroughly addressed in [2], [4], would require significantly higher values of the control inputs to be vanished than those of the chaotic ones. The considerable control inputs expectedly result in the higher driving magnetic torques than the ones used in the network subject to the chaotic dynamics (Fig. 7(b)). The two phases of the control process, which we discussed for the chaotic case, can be observed for the hyperhcaotic one such that the oscillatory negative control inputs/driving magnetic torques suppress the hyperchaotic dynamics. Note that the green boxes shown in Figs. 7(a) and 7(b) reveal the incremental values of the control inputs/torques to rotate the valves to the desirable trajectories.

Shown in Fig. 8(a) are both the upstream and downstream valves' rotation angles revealing that the valves' motions tend to the desirable trajectories (Eq. 17). Figs. 8(b) and 8(c) present the convergence of both the error and combined tracking error signals to zero, respectively. Consequently, it is straightforward to conclude that the adaptation and

control laws guarantee both the global stability of the coupled network and convergence of the tracking errors in which we analytically discussed in Section 3.

V. Conclusions

In this paper, we represented the interconnected sixth-order dynamic model of the network of two bi-directional solenoid actuated butterfly valves subject to the sudden contraction. The network undergoes the coupled chaotic and hyperchaotic dynamics for a set of initial conditions, the Initial_1 and Initial_2, and critical parameters. The adaptation and control laws were developed to vanish the chaotic/hyperchaotic dynamics and then push the dynamically coupled valves to track the desirable trajectories.

For the initial conditions resulted in the chaotic/hyperchaotic dynamics, we revealed that the downstream set required the higher control inputs/driving magnetic torques than those of the upstream one. The two phases of the control process were also distinguished to vanish the chaotic/hyperchaotic dynamics in addition to mitigating the harmful effects of the hydrodynamic torque (as a helping load) which expectedly magnifies the amplitude of dangerous stochastic oscillation. The first phase by presenting the oscillatory negative control inputs removed the chaotic/hyperchaotic dynamics. The control inputs of the second phase gradually took the positive values to push the valves to the desirable trajectories. The control inputs of the downstream set were shown to be higher than those of the upstream one, for the second phase of both the chaotic and hyperchaotic cases, in order to overcome the higher resistance bearing torque. We have previously established that the bearing torque of the downstream set with a smaller pipe diameter is higher than that of the upstream one.

References

[1] P. Naseradinmousavi, H. Ashrafiuon, and M. A. Ayoubi, "An adaptive centralized approach to control chaotic and hyperchaotic dynamics of smart valves network," *ASME Journal of Computational and Nonlinear Dynamics*, vol. 13, no. 1, pp. 011 002–011 002–11, 2018.

[2] P. Naseradinmousavi, D. B. Segala, and C. Nataraj, "Chaotic and hyperchaotic dynamics of smart valves system subject to a sudden contraction," *ASME Journal of Computational and Nonlinear Dynamics*, vol. 11, no. 5, pp. 051 025–051 025–9, September 2016.

[3] P. Naseradinmousavi, M. Krstic, and C. Nataraj, "Design optimization of dynamically coupled actuated butterfly valves subject to a sudden contraction," *ASME Journal of Mechanical Design*, vol. 138, no. 4, pp. 041 402–041 402–11, April 2016.

[4] P. Naseradinmousavi, S. G. Machiani, M. A. Ayoubi, and C. Nataraj, "Coupled operational optimization of smart valve system subject to different approach angles of a pipe contraction," *Journal of Structural and Multidisciplinary Optimization*, vol. 55, no. 3, pp. 1001–1015, March 2017.

[5] P. Naseradinmousavi, "A novel nonlinear modeling and dynamic analysis of solenoid actuated butterfly valves coupled in series," *ASME Journal of Dynamic Systems, Measurement, and Control*, vol. 137, no. 1, pp. 014 505–014 505–5, January 2015.

[6] P. Naseradinmousavi and C. Nataraj, "Optimal design of solenoid actuators driving butterfly valves," *ASME Journal of Mechanical Design*, vol. 135, no. 9, pp. 094 501–094 501–5, July 2013.

[7] ——, "Transient chaos and crisis phenomena in butterfly valves driven by solenoid actuators," *Journal of Communications in Nonlinear Science and Numerical Simulation*, vol. 17, no. 11, pp. 4336–4345, November 2012.

[8] D. Lee, P. Naseradinmousavi, and C. Nataraj, "Nonlinear model-based adaptive control of a solenoid-valve system," *Journal of Control Science and Engineering*, vol. 2012, 2012.

[9] P. Naseradinmousavi and C. Nataraj, "Nonlinear mathematical modeling of butterfly valves driven by solenoid actuators," *Journal of Applied Mathematical Modelling*, vol. 35, no. 5, pp. 2324–2335, 2011.

[10] P. Naseradinmousavi, M. Bagheri, H. Ashrafiuon, M. Canova, and D. B. Segala, "Suppressing chaotic/hyperchaotic dynamics of smart valves network using decentralized and centralized schemes," in *the ASME 2017 Dynamic Systems and Control Conference*, vol. 3, no. DSCC2017-5006, Tysons Corner, Virginia, USA, October 11-13 2017, p. V003T42A00.

[11] P. Naseradinmousavi, M. Krstic, M. Bagheri, and C. Nataraj, "Coupled chaotic and hyperchaotic dynamics of actuated butterfly valves operating in series," in *The ASME 2016 Dynamic Systems and Control Conference*, vol. 2, no. DSCC2016-9601, Minneapolis, Minnesota, USA, October 12-14 2016, p. V002T17A001.

[12] P. Naseradinmousavi, M. Bagheri, and C. Nataraj, "Coupled operational optimization of smart valve system subject to different approach angles of a pipe contraction," in *The ASME 2016 Dynamic Systems and Control Conference*, vol. 1, no. DSCC2016-9627, Minneapolis, Minnesota, USA, October 12-14 2016, p. V001T02A001.

[13] P. Naseradinmousavi and C. Nataraj, "Design optimization of solenoid actuated butterfly valves dynamically coupled in series," in *Proceedings of the ASME 2015 Dynamic Systems and Control Conference*, vol. 2, no. DSCC2015-9605, October 2015, p. V002T33A001.

[14] P. Naseradinmousavi, "Optimal design of solenoid actuated butterfly valves dynamically coupled in series," in *Proceedings of the ASME 2015 International Mechanical Engineering Congress & Exposition*, vol. 4A: Dynamics, Vibration, and Control, no. IMECE2015-50094, Houston, November 13-19 2015, p. V04AT04A032.

[15] P. Naseradinmousavi and C. Nataraj, "A chaotic blue sky catastrophe of butterfly valves driven by solenoid actuators," in *Proceedings of the ASME 2011 International Mechanical Engineering Congress & Exposition*, vol. 7: Dynamic Systems and Control; Mechatronics and Intelligent Machines, Parts A and B, no. IMECE2011/62608, November (11-17) 2011, pp. 25–31.

[16] C.-W. Chang-Jian, "Gear dynamics analysis with turbulent journal bearings mounted hybrid squeeze film damper-chaos and active control analysis," *ASME Journal of Computational and Nonlinear Dynamics*, vol. 10, no. 1, pp. 011 011–011 011–11, 2014.

[17] C. Morel, R. Vlad, and J.-Y. Morel, "Anticontrol of chaos reduces spectral emissions," *ASME Journal of Computational and Nonlinear Dynamics*, vol. 3, no. 4, pp. 041 009–041 009–6, 2008.

[18] D. Chen and W. Liu, "Chaotic behavior and its control in a fractional-order energy demand-supply system," *ASME Journal of Computational and Nonlinear Dynamics*, vol. 11, no. 6, pp. 061 010–061 010–7, 2016.

[19] B. Wang, K. Shi, C. Zhang, and D. Zhu, "Fuzzy generalized predictive control for nonlinear brushless direct current motor," *ASME Journal of Computational and Nonlinear Dynamics*, vol. 11, no. 4, pp. 041 004–041 004–7, 2015.

[20] R. Luo and Y. Zeng, "The control and synchronization of a class of chaotic systems with output variable and external disturbance," *ASME Journal of Computational and Nonlinear Dynamics*, vol. 11, no. 5, pp. 051 011–051 011–7, 2015.

[21] B. S. Reddy and A. Ghosal, "Asymptotic stability and chaotic motions in trajectory following feedback controlled robots," *ASME Journal of Computational and Nonlinear Dynamics*, vol. 11, no. 5, pp. 051 012–051 012–11, 2015.

[22] P. Khamsuwan and S. Kuntanapreeda, "A linear matrix inequality approach to output feedback control of fractional-order unified chaotic systems with one control input," *ASME Journal of Computational and Nonlinear Dynamics*, vol. 11, no. 5, pp. 051 021–051 021–7, 2016.

[23] M. Krstić, I. Kanellakopoulos, and P. Kokotović, *Nonlinear and Adaptive Control Design*. Wiley-Interscience, 1995.

[24] Slotine and Li, *Applied Nonlinear Control*. Prentice-Hall, 1991.